Model-Based Fitting of EEG Signals with Uncertainty Quantification for Robust Alpha Wave Identification

Valentina Casadei, *Student Member, IEEE*, and Roberto Ferrero, *Senior Member, IEEE*

***Abstract*—Electroencephalography is a non-invasive technique widely used to assess the brain's electrical activity, suitable for a variety of applications in clinical and non-clinical environments. However, the reliable identification of specific EEG features still remains a challenge, especially if the signals are recorded from wearable devices, notably less accurate than their hospital counterparts. The uncertainty analysis can help to address this challenge, by providing a robust and rigorous tool to assess the validity of the information extracted from the signals. This is particularly important in automated processes (such as brain-machine interfaces), to avoid misclassifications and misinterpretation. This paper proposes the use of a model-based fitting of pre-filtered EEG signals, combined with uncertainty quantification, to extract the alpha amplitude oscillation with an optimal trade-off between accuracy and time resolution and, importantly, to allow the identification of those parts of the signal that do not follow the expected alpha dynamics, e.g. because affected by artifacts. This is achieved through a metrology-sound analysis of compatibility between measurement and model, taking their respective uncertainties into consideration. The proposed method has been successfully tested on real EEG signals and shown to have significant advantages in terms of time resolution and interpretability, compared to more traditional techniques, such as the ICA by temporal decorrelation, especially when applied to single-channel signals.**

***Index Terms*—Electroencephalography, Biomedical measurement, Signal processing, Time-domain analysis, Measurement uncertainty, Parameter estimation, Wearable sensors**

I. Introduction

Electroencephalography (EEG) is a non-invasive method of recording the brain's electrical activity through electrodes attached to the scalp in well-defined positions, typically according to the 10-20 system [1]. The wealth of information available within the electroencephalography signals (EEGs) has made them suitable to be implemented in several applications, clinical and non-clinical [2]. In clinical applications, most specifically in neurology, EEGs provide real-time insight into the mental state of the patient, therefore helping with the diagnosis of conditions or brain structure abnormalities, such as epilepsy, dyslexia, seizures, post-traumatic stress disorder, Attention Deficit Hyperactivity Disorder (ADHD) and mental fatigue, to name a few. In non-clinical applications, EEGs provide instructions to be translated into control commands for an external device, as part of Brain-Computer Interfaces (BCI), or more generically Brain-Machine Interfaces (BMI), e.g. to assist people with language or movement impairment [3].

Although EEG opened to several promising applications over the years [4], there are still important challenges to address, in particular regarding the accuracy and reliability of extracted features, especially when using wearable devices, which are notably less accurate than their hospital counterparts. EEGs are weak bio-electrical signals, characterized by a very low amplitude (usually less than 100 μV), which makes them prone to record artifacts from other electrophysiological activities of the body, such as muscular, ocular, and cardiac. In addition, EEGs are characterized by a fast dynamic, changing in both amplitude and frequency content over time, due to mental state transitions. Because of the above challenges, the supervision of a trained clinician is recommended for a correct interpretation of the signals; however, this is not feasible in non-clinical applications, where more automated tools are required.

This paper aims to contribute to addressing the challenge of correctly identifying EEG features in automated applications, focusing on a notable example, i.e. the measurement of alpha activity, defined within the [8 14] Hz frequency range and associated to relaxed and meditation mental states. The alpha activity is one of the most investigated EEG features, in both clinical [5] and non-clinical studies [6], because of its distinctive characteristics and relatively easy interpretation; nevertheless, a reliable and robust identification of alpha waves remains challenging. Commonly, during the pre-processing phase, alpha information is extracted through band-pass filters in the frequency range of interest; however, the filter bandwidth must be large enough to preserve the amplitude oscillation, leading to two challenges: 1) the accurate estimation of the time-varying amplitude, 2) the discrimination between alpha activity and artifacts, which may look similar to each other after being filtered. These challenges are particularly critical for applications that rely on an accurate alpha amplitude (or power) estimation over short timescales, e.g. to analyze the alpha dynamics in response to fast stimuli in a cognitive task [7].

While there is a vast literature on denoising and signal processing techniques to remove artifacts and extract signal features, there is an important gap in metrology-sound tools able to provide a confidence level for the automated identification of alpha activity in each time window of the signal. Moreover, many techniques work better (or only) with a large

V. Casadei and R. Ferrero are with the Department of Electrical Engineering and Electronics, University of Liverpool, Liverpool L69 3GJ, UK (e-mail: Valentina.Casadei@liverpool.ac.uk, Roberto.Ferrero@liverpool.ac.uk).
This work was partially supported by the Hugh Greenwood Legacy for Children's Health Research.

number of EEG signals and, therefore, are not suitable for wearable devices using a limited number of channels, or even only one.

Among denoising techniques, Independent Component Analysis (ICA), a Blind Source Separation (BSS) method, is arguably the most used one (implemented also in the EEGLAB MatLab Toolbox for example [8]) to separate different sources within the signal, including artifacts [9]. In the traditional ICA, a number of sources equal to or less than the number of channels are separated, without requiring any previous knowledge about them [10]; however, solutions to apply the ICA to single channels have been proposed too [11], [12]. Other variations of ICA include the ICA by temporal decorrelation (described in Sec. VIII), Wavelet-ICA and a combination of singular spectral analysis and ICA (SSA-ICA [13]). However, Wavelet-ICA depends on the wavelet window of analysis, which requires a priori knowledge of the signals [14], and in SSA-ICA, even though the spectral analysis is applied recursively on the single channel to extract several components in high and low frequencies, the decomposition is defined by a manually selected threshold, therefore it is not suitable for online or fully automated applications [15].

Along with BSS, the Joint Blind Source Separation (JBSS) methods also consider similar dependence across the data, and are specifically implemented for muscular artifacts removal [16]. Among them, independent vector analysis (IVA) can be treated as an extension of ICA, as it decomposes the components into independent sources while exploiting the dependence among the data [17], [18].

Kalman filter has also been applied as a denoising technique, but its computation may be too complex for some applications and, in some cases, the reliability of the estimated EEG signals requires further investigation [19].

Following denoising, the challenge of estimating a time-varying amplitude still exists, for which different processing methods can be used, in the time, frequency or time-frequency domains [20], [21]. Classic frequency-domain techniques, such as the Fourier Transform, are designed for periodic signals, while EEGs are non-periodic: this leads to errors in the amplitude estimation which would impact the reliability of the classification, especially in presence of artifacts, because the Fourier Transform requires a synchronous window length of analysis to avoid spectral leakage. On the one hand, to overcome the leakage problem, time and time-frequency domain methods have been developed, such as Hilbert, Taylor-Fourier, and wavelet transforms [22]–[24]. On the other hand, they could be too complex and even not useful in some circumstances, and their results may hinder a physical interpretation. Wavelet transform is used to decompose the signal into components based on frequency bands, which may be useful for a complete EEG signal [25], but the alpha oscillation is well defined within a narrow frequency range, therefore it would not be effective in this case. Hilbert transform has been proved to be useful if applied on signals with time-varying main frequency, while the alpha frequency is only slightly modulated around a constant value. Lastly, Taylor-Fourier transform can be successfully applied on signals characterized by time-varying harmonics, while the alpha band oscillation is almost sinusoidal.

Machine Learning (ML) and statistic techniques have become widely used due to their ability in dealing with a larger amount of data [26], providing an accurate and efficient classification of the information within EEG [27]. However, ML is not able to detect which specific part of the signal truly carries the information of interest (i.e. alpha information), leading to possible misclassifications [28].

Among alternative approaches, it is worth mentioning the use of entropy applied on EEG signals for the quantification of similarity among different patterns in either time or frequency domains, without any previous knowledge of the signals [29], [30]. However, there appear to be quantitative differences in defining the same mental states, causing a limitation for practical performance [31].

Within the aforementioned denoising and signal processing literature, an important gap that emerges is the lack of an uncertainty analysis associated with the amplitude estimation and the presence of artifacts. Indeed, there is an important difference between estimating the expected accuracy of a method based on some statistical analysis on large data sets, as most works in the literature do, and the estimation of the uncertainty of each result. According to international measurement standards [32], uncertainty is a fundamental parameter that should be added to every measurement result for a correct interpretation, and it is particularly important for measurements obtained from wearable devices, which are likely to be affected by significant uncertainty sources of different types [33]–[35], many of which are largely variable and/or unpredictable. A notable example is the automated feature extraction in BCI applications, where uncertainty analysis is essential to guarantee the reliability of the unsupervised decision-making process, but, more generally, uncertainty is important every time measurement results are compared to each other or to a threshold, to determine whether there is a significant difference between them or not; examples of applications include the analysis of post-error behavior in cognitive tasks [7], the detection of cognitive disorders [27] and the assessment of driving performance [36], to name a few.

In this work, a time-domain model-based method for EEG signal fitting, previously introduced in [37], is used to estimate the time-varying amplitude of the alpha wave, in combination with a rigorous evaluation of the model and measurement uncertainties affecting the amplitude estimation. The uncertainty analysis, which is the core contribution of this paper, enables a metrology-sound definition of compatibility between the measured signal and its model-based reconstruction from the estimated parameters, which, in turn, provides a level of confidence about the genuine alpha nature of the signal in question.

The proposed method provides some unique advantages, especially for applications that require or benefit from a short time resolution: 1) an optimal window of analysis, tailored to each subject's main alpha frequency and other signal features, derived from the uncertainty minimization; 2) the estimation of the alpha amplitudes with an optimal trade-off between accuracy and time resolution, on sub-cycle time

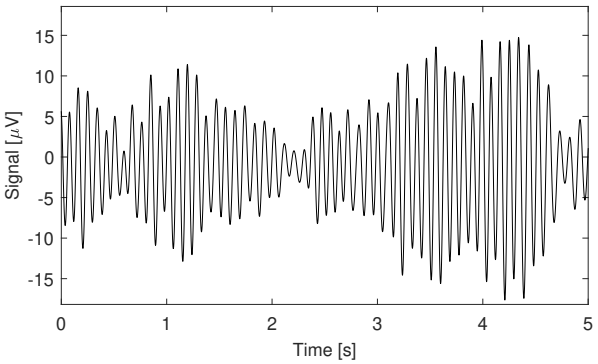

Fig. 1. Example of alpha wave activity recorded from a healthy subject.

windows (i.e., shorter than a full cycle of the alpha wave); 3) the possibility to assess the window-by-window compatibility between the measured signal and the model used for the parameter estimation, which allows the detection of artifacts or other non-alpha components in the signal, such as head or ocular movements. However, the method is general, and it is presented on purpose without emphasizing the details of any specific application: the key aspects of the method are a simple model of the alpha wave, whose validity does not depend on a particular experimental setup, and the analysis of measurement and model uncertainties, which are always possible, and indeed recommended, in any application.

II. Alpha Wave Model-Based Identification

EEG can be subdivided into several sub-bands (delta, theta, alpha, beta, gamma) according to specific frequency ranges. Each sub-band refers to a different brain activity and can be extracted from the raw signal by applying a band-pass filter in the frequency range of interest; hence, to extract the alpha information, a filter is typically applied within the [8 14] Hz range, leading to a signal like the example shown in Fig. 1. The signal is characterized by a clear oscillation at the alpha frequency, with noticeable amplitude variations on timescales of seconds or slightly shorter. Mathematically, the alpha wave can be generically described as a sinusoidal signal with time-varying amplitude $A_\alpha(t)$, phase $\varphi_\alpha(t)$ and frequency $\omega_\alpha(t) = 2\pi f_\alpha(t)$:

$$s_\alpha(t) = A_\alpha(t)\sin\left(\omega_\alpha(t)t + \varphi_\alpha(t)\right) \tag{1}$$

Since the alpha frequency does not change significantly over time within the same subject [38], it can be estimated on the whole signal and considered as a constant and known value. Therefore, (1) can be written as:

$$s_\alpha(t) = A_\alpha(t)\sin\left(\omega_\alpha t + \varphi_\alpha(t)\right) \tag{2}$$

However, it is worth noting that (2) still refers to a general model, since the argument of the sine is still a generic function of time, and the signal is still non-periodic because $A_\alpha(t)$ and $\varphi_\alpha(t)$ are generally non-periodic oscillations.

Equation (2) can be used to estimate the time-varying amplitude and phase from a measured filtered signal. $A_\alpha(t)$ and $\varphi_\alpha(t)$ are characterized by limited dynamics, as shown in Fig. 1, due to two main reasons: 1) physiological [38] and 2) the application of the band-pass filter, which acts as a low-pass filter on the amplitude and phase modulations. Therefore, $A_\alpha(t)$ and $\varphi_\alpha(t)$ can be assumed as constants in a limited time interval, whose values can be estimated window by window. Each window has a length $L \cdot t_s$, where L is the number of samples and t_s is the sampling time of the original signal. Choosing a local time axis with the origin in the center of the window, the discrete-time model becomes:

$$m_{\alpha_n}(l \cdot t_s) = A_n \sin(\omega_\alpha(l \cdot t_s) + \varphi_n) \tag{3}$$

where $l = -\frac{L-1}{2}, ..., \frac{L-1}{2}$ is the discrete time index, $n = 1, ..., N$ is the window index, being N the total number of windows, while A_n and φ_n are the parameters to be estimated.

Although, theoretically, A_n and φ_n could be estimated in both time and frequency domains, a time-domain approach is more appropriate here because it does not require the window length to be an integer multiple of the signal period and, therefore, it provides more flexibility in the choice of the window length (especially sub-cycle) and more robustness in case of inaccurate alpha frequency estimation.

In the time domain, the estimation of A_n and φ_n can be performed analytically, more conveniently by introducing the variables K_{1_n} and K_{2_n}, which are functions of A_n and φ_n, defined as:

$$\begin{aligned} K_{1_n} &= A_n \cos(\varphi_n) \\ K_{2_n} &= A_n \sin(\varphi_n) \end{aligned} \tag{4}$$

Therefore, (3) in matrix form becomes:

$$m_{\alpha_n}(l \cdot t_s) = \begin{bmatrix} \sin(\omega_\alpha(l \cdot t_s)) & \cos(\omega_\alpha(l \cdot t_s)) \end{bmatrix} \cdot \begin{bmatrix} K_{1_n} \\ K_{2_n} \end{bmatrix} \tag{5}$$

where the first matrix is constant and known, while $\mathbf{K}_n$ is the vector of the parameters to be estimated.

Equation (5) is linear and can be written in the more compact form:

$$m_{\alpha_n} = \mathbf{C} \cdot \mathbf{K}_n \tag{6}$$

Since matrix $\mathbf{C}$ is not invertible, the least square method is implemented to obtain the best estimate for $\mathbf{K}_n$ from the filtered signal in each window:

$$\mathbf{K}_{e_n} = \mathbf{D} \cdot s_{filtered_n} \tag{7}$$

where $s_{filtered_n}$ is the filtered signal and $\mathbf{D}$ is the pseudo-inverse matrix of $\mathbf{C}$:

$$\mathbf{D} = (\mathbf{C}^T \cdot \mathbf{C})^{-1} \cdot \mathbf{C}^T \tag{8}$$

Finally, A_{e_n} and φ_{e_n} can be derived as:

$$A_{e_n} = \sqrt{K_{1_{e_n}}^2 + K_{2_{e_n}}^2} \tag{9}$$

$$\varphi_{e_n} = \begin{cases} \arctan\left(\frac{K_{2_{e_n}}}{K_{1_{e_n}}}\right), & K_{1_{e_n}} > 0 \\ \arctan\left(\frac{K_{2_{e_n}}}{K_{1_{e_n}}}\right) + \pi, & K_{1_{e_n}} < 0 \\ \frac{\pi}{2}\mathrm{sgn}\left(K_{2_{e_n}}\right), & K_{1_{e_n}} = 0 \end{cases} \tag{10}$$

It is important to note that the standard least-square method presented in this section will always allow obtaining amplitude

and phase estimates in each window, regardless of whether the window contains a genuine alpha signal that satisfies the model assumptions above or not. It is therefore essential to add a validation step, to ensure that the estimated parameters are used in a meaningful way by any application relying on them, whether clinical, BCI, or other. The solution proposed in this paper is a metrology-sound approach, based on the fundamental measurement science concepts of uncertainty and compatibility: a genuine alpha signal will have to be compatible with its model-based reconstruction from the estimated parameters, taking their respective uncertainties into consideration. This type of compatibility analysis requires not only an accurate uncertainty analysis but also the estimation of the signal parameters with the lowest possible uncertainty, to maximize the discrimination ability of the method. The uncertainty evaluation and its minimization through the choice of an optimal window length L will be thoroughly discussed in Secs. IV and V, after presenting the experimental method used in this work in Sec. III.

III. Experimental Method

For the purpose of illustrating and testing the proposed method, signals have been recorded from two healthy subjects, using a wireless EEG wearable device, the Neuroelectrics Enobio 8-channels; the attribute 'wearable' is used here to signify that the entire system, including the acquisition unit, is on the head, with no wired connections to any external device, so the user's ability to move is not affected. All recordings are performed in a still condition to avoid muscular artifacts as much as possible, with closed and open eyes, while the subject remains in a relaxed state. The electrodes used are gel-based and are placed in the following positions of the 10-20 system: O1, O2, T7, T8, C3, C4, Fz, and Cz. The signals are recorded with a ground reference electrode placed on the ear, while Fz is chosen as the reference electrode for the definition of differential signals used for the processing.

All signals are sampled with 500 Hz sampling frequency and 24 bit resolution (50 nV), and the acquisition unit has a bandwidth from 0 to 125 Hz. The noise level arising from the acquisition device is expected to be less than 1 μV, according to the manufacturer. It should be noted that this noise level does not include other noise or disturbance that is likely to affect EEG signals, arising either from the non-EEG electrical activity of the human body or from the skin-electrode interface, which can be higher than the intrinsic noise of the acquisition device. The unpredictable presence and amplitude of such noise (used here in its broadest meaning) are the reason why the compatibility analysis presented in this paper is required, as explained above.

The differential signals are firstly filtered by a 5$^{\text{th}}$ order Butterworth IIR high-pass filter, with a -1 dB cut-off frequency at 0.1 Hz, to remove possible large components at very low frequencies (e.g., slowly drifting offset). Then, the signals are filtered by a 150$^{\text{th}}$ order FIR band-pass filter in the [8 14] Hz range, to extract the alpha band. The frequency responses of both filters are shown in Fig. 2. The IIR filter has a negligible effect on the extracted alpha signal, as its maximum

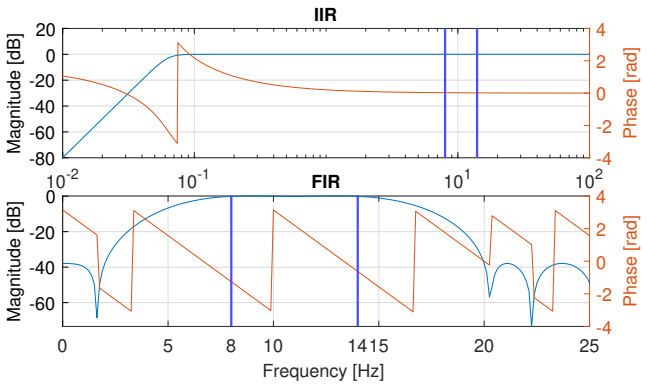

Fig. 2. Frequency responses of the IIR (top) and FIR (bottom) filters applied to the raw EEG signal. The vertical lines mark the alpha band, [8 14] Hz.

magnitude variation and phase shift in the alpha band are less than 0.01 dB (0.1 %) and 1.5°, respectively. Similarly, the maximum magnitude variation caused by the FIR filter in the alpha band is less than $\pm$0.09 dB ($\pm$1 %), which is negligible too. On the other hand, the phase shift introduced by the FIR filter is much more significant, but it is proportional to frequency in the pass band, so it corresponds to a constant delay of 0.15 s, which can be easily compensated in offline processing without causing any distortion to the signal; this is actually one of the main reasons for choosing an FIR filter over an IIR in this application (see [37] for more details on the design rationale for this filter).

IV. Uncertainty Estimation

As explained in Sec. II, in order to ensure good reliability to any application relying on the estimated alpha wave parameters, the evaluation of their uncertainties is essential for measurement-model compatibility verification. This is required to validate each individual result, on a short timescale, rather than validating the measurement method as a whole, through a statistical analysis. The adopted approach is illustrated here focusing on the amplitude parameter, but a similar procedure is applied to the phase too.

From (7), two sources of uncertainties are identified: 1) the measurement noise, affecting the acquired signal ($s_{filtered}$) and 2) the model approximations, introduced when assuming constant parameters in each window. These two sources are independent of each other and therefore can be combined into a total uncertainty, according to the standard rule for the combination of uncorrelated uncertainty contributions [32]:

$$u(A_e)_{tot} = \sqrt{u(A_e)^2_{meas} + u(A_e)^2_{model}} \tag{11}$$

where $u(A_e)_{meas}$ refers to the measurement uncertainty contribution and $u(A_e)_{model}$ to the model one. The subscript n has been dropped here for compactness of notation.

In this section, both uncertainties will be described and analyzed thoroughly, highlighting their dependence on the window length L. The results are shown considering f_α = 11 Hz, but different frequency values lead to similar results.

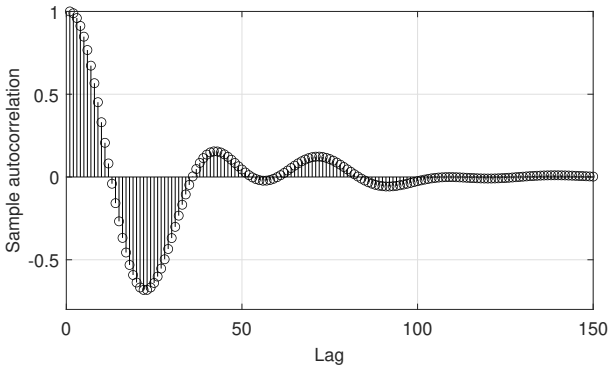

Fig. 3. Auto-correlation of white noise filtered by the band-pass filter described in Sec. III.

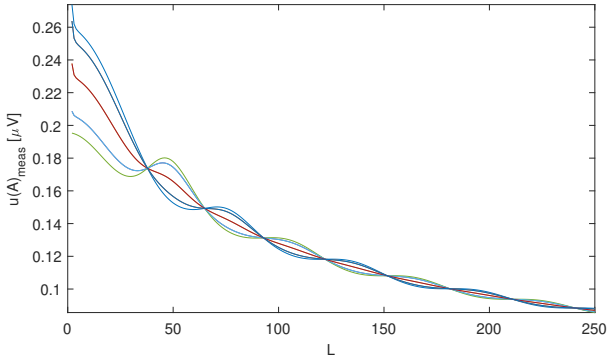

Fig. 4. Relationship between $u(A)_{meas}$ and the window length, for f_α = 11 Hz. The curves refer to different values of φ_e, defined in the interval $[0\ \pi]$ with $\pi/8$ step.

A. Measurement uncertainty

The measurement uncertainty can be quantified assuming that the raw signal is affected by a white noise, characterized by a variance σ_w^2, which can be estimated from the specifications provided by the manufacturer (the upper limit $\sigma_w = 1\ \mu$V is used here). According to (7), the $\mathbf{K}_e$ estimation comes from the filtered signal: thus, the white noise is filtered by the band-pass filter as well, which introduces a strong correlation between noise samples. Therefore, the filtered noise is described by a full covariance matrix $\mathbf{\Sigma}_s$, which can be estimated numerically from the auto-correlation function of simulated noise, shown in Fig. 3. The propagation of $\mathbf{\Sigma}_s$ through (7) is given by:

$$\mathbf{\Sigma}_{K_e} = \mathbf{D} \cdot \mathbf{\Sigma}_s \cdot \mathbf{D}^T \tag{12}$$

Since the window is symmetric with respect to the time axis, $\mathbf{\Sigma}_{K_e}$ becomes diagonal, i.e. K_{1_e} and K_{2_e} are uncorrelated:

$$\mathbf{\Sigma}_{K_e} = \begin{bmatrix} \sigma^2_{K_{1_e}} & 0 \\ 0 & \sigma^2_{K_{2_e}} \end{bmatrix} \tag{13}$$

Thus, the propagation of $\mathbf{\Sigma}_{K_e}$ over the amplitude estimation (9) is given by:

$$\begin{aligned} u(A_e)^2_{meas} = \\ &= \left(\frac{\partial A_e}{\partial K_{1_e}}\right)^2 \cdot \sigma^2_{K_{1_e}} + \left(\frac{\partial A_e}{\partial K_{2_e}}\right)^2 \cdot \sigma^2_{K_{2_e}} = \\ &= \cos^2(\varphi_e) \cdot \sigma^2_{K_{1_e}} + \sin^2(\varphi_e) \cdot \sigma^2_{K_{2_e}} \end{aligned} \tag{14}$$

Equation (14) reveals that $u(A_e)_{meas}$ depends on the window length L (through $\mathbf{\Sigma}_{K_e}$) and on φ_e (with period π). Of these two parameters, only the window length can be controlled when sectioning the signal, whereas the phase can be treated as a random variable, so the uncertainty is analyzed here as a function of the window length only, as shown in Fig. 4.

Similar curves are obtained for different ω_α values and lead to the general conclusion that longer window lengths correspond to lower measurement uncertainties. Fig. 4 shows that the phase value has little effect on the uncertainty, so a mean curve can be used to determine the optimal window length. However, the optimal length should be chosen considering also the contribution of the model uncertainty on the amplitude estimation.

B. Model uncertainty

The model uncertainty arises from the simplification introduced in the model (3), used for the amplitude and phase estimation, which approximates the time-varying $A_\alpha(t)$ and $\varphi_\alpha(t)$ in (2) with constant parameters in each window. Such a simplification is unavoidable because the amplitude and phase variations in time are generally unknown and cannot be included in the model. However, their bandwidths are known to be limited, as explained in Sec. II. As a consequence, it is possible to describe the signal dynamics for $A_\alpha(t)$ and $\varphi_\alpha(t)$ in terms of band-limited random signals, with specific models for amplitude and phase, which can be used for the uncertainty quantification.

The models can be identified from real EEG signals, evaluating how the amplitude and phase change over a timescale of several seconds or a few minutes and extrapolating the dynamics on shorter timescales from those results. Examples of amplitude and phase spectra thus obtained are illustrated in Fig. 5. The amplitude dynamic can be modeled as a white random signal filtered by a first-order low-pass filter, with a cut-off frequency of around 1 Hz. On the other hand, the phase dynamic is better described by the integral of a white random signal, without a visible band limit in the considered range (here up to 5 Hz). A first-order low-pass behavior can still be assumed, with a cut-off frequency close to the band limit of the measured spectra; hence, the phase dynamic is modeled as the integral of a white random signal filtered by a first-order low-pass filter, with a cut-off frequency around 5 Hz. The model parameters are identified for each subject from a calibration signal.

In order to quantify the error in the parameters estimation, a Monte Carlo algorithm is implemented to simulate amplitude and phase modulations, based on the block diagrams shown in Fig. 6. In more detail, the amplitude variation $\tilde{A}(t)$ is built around A_0, which is the mean of all the estimated amplitudes values obtained from the calibration signal; on the other hand, the phase variation $\tilde{\varphi}(t)$ is built around a

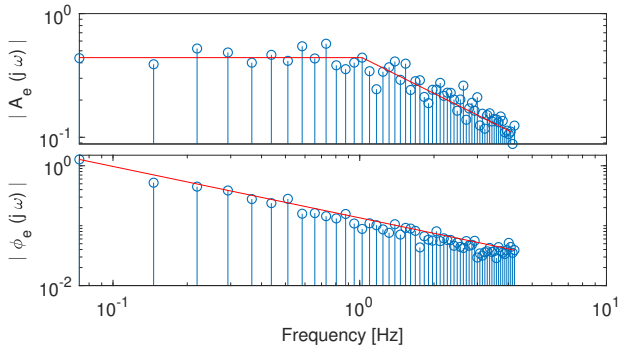

Fig. 5. Typical example of A_e and φ_e spectra, experimentally obtained from real EEG signals.

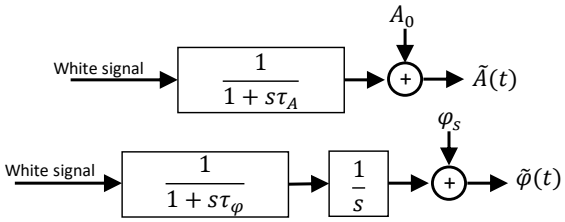

Fig. 6. Block diagrams used to model the amplitude and phase dynamics in the Monte Carlo simulation.

random variable φ_s. On each generated signal, the amplitude and phase are estimated using the alpha model, and the mean and standard deviation of the estimation errors are used to define the systematic error and uncertainty, respectively, as shown in (15) and in Fig. 7 for the amplitude:

$$\begin{aligned} e(A_e)_{model} &= \mu(A_e - \mu(\tilde{A}(t)) \\ u(A_e)_{model} &= \sigma(A_e - \mu(\tilde{A}(t)) \end{aligned} \tag{15}$$

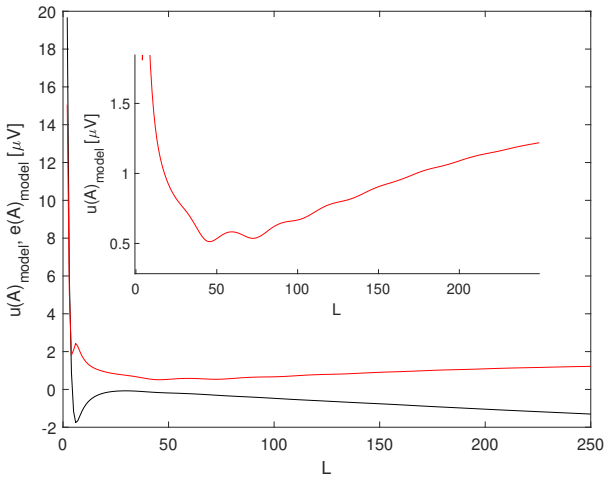

Fig. 7. Amplitude model uncertainty $u(A)_{model}$ (red line), for f_α = 11 Hz, with the minimum of the function highlighted in the box, and the systematic error (black line).

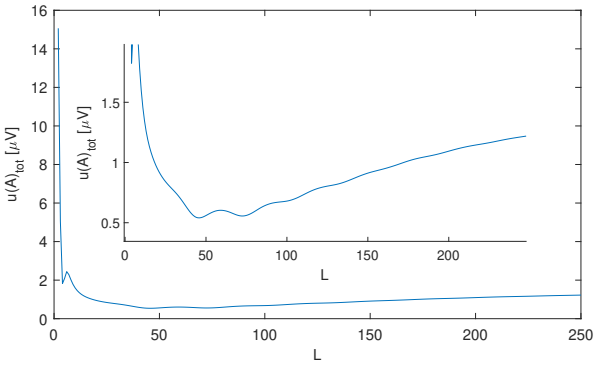

Fig. 8. Total amplitude uncertainty $u(A)_{tot}$, for f_α = 11 Hz, with the minimum of the function highlighted in the box.

Similarly to the measurement uncertainty (in Fig. 4), the model uncertainty has very large values for very small window lengths, but it also increases again at longer window lengths, whereas the measurement uncertainty decreases almost monotonically.

It is worth noting that the systematic error is not always negligible, but it can be compensated by subtracting it from the estimated values of both parameters, if necessary, thus it will not be further discussed.

V. Uncertainty Minimization

The uncertainty analysis described in the previous section is applied to the signal analysis with a double aim: first, it is used to determine the optimal window length for each signal (or each set of signals in similar conditions), based on the expected alpha frequency and the expected dynamics of amplitude and phase; then, once the amplitude and phase have been estimated window by window, it is used to evaluate the uncertainty of each estimate.

A. Determination of the optimal window length

Choosing an optimal window length for each signal, or for a set of signals acquired from the same subject, allows for a tailored analysis that can better adapt to the non-stationary nature of EEG and is expected to lead to more accurate results, according to the uncertainty analysis reported above. The amplitude uncertainty minimization is chosen as the optimization goal, since the amplitude is the parameter of interest for the alpha oscillation identification, within this research. Thus, the optimal window length L_{opt} is the value that minimizes the total amplitude uncertainty, introduced in (11) and represented in Fig. 8. It is worth noting that there could be more than one local minimum within the same function: if the uncertainty values in the local minima are similar to each other, the smallest window length is to be preferred in order to provide a better time resolution in the amplitude estimation.

B. Look-up table of uncertainty values

Once the optimal window length has been identified, a more accurate estimation of the amplitude and phase uncertainties

can be calculated as a function of the estimated values of amplitude and phase in each window. Since the calculation requires a Monte Carlo simulation, it is not practical to repeat it for each window during the processing of each signal; instead, the calculation is done once for a fixed set of amplitude and phase values and the results are stored in a look-up table for future use. The simulation is based again on the models described in the previous section, but with defined values for amplitude and phase within the ranges [1 250] μV and [0 2π] rad, with steps of 1 μV and 0.1 rad, respectively. This amplitude range is likely to include all possible amplitude values of real alpha signals, according to the literature.

VI. Compatibility Analysis

The model-based estimation method, with the associated uncertainty analysis, offers the main advantage of providing the possibility to verify if the estimated values are compatible with the model assumptions, by checking if the reconstructed signal from the estimated parameters is compatible with the measured signal, taking their uncertainties into account.

A. Signal reconstruction

Once the amplitude and phase parameters have been estimated in each window, with the optimal length L_{opt}, the signal can be reconstructed within the window, using the model explained in Sec. II, in particular (3):

$$s_e(t) = s_e(l \cdot t_s) = A_e \sin(\omega_\alpha (l \cdot t_s) + \varphi_e) \tag{16}$$

The previous section explained how to calculate the uncertainties of amplitude and phase separately; here, they have to be propagated over the signal reconstruction and combined with the model uncertainty associated with the reconstruction itself. The measurement and model contributions are first evaluated separately using different mathematical approaches and then combined.

The total measurement uncertainty propagation over the reconstructed signal is performed analytically from (5):

$$\begin{aligned} u\left(s_e(t)\right)^2_{meas} = \\ &= \left(\frac{\partial m_\alpha}{\partial K_1}\right)^2 \cdot \sigma^2_{K_{1_e}} + \left(\frac{\partial m_\alpha}{\partial K_2}\right)^2 \cdot \sigma^2_{K_{2_e}} = \\ &= \sin^2(\omega_\alpha t) \cdot \sigma^2_{K_{1_e}} + \cos^2(\omega_\alpha t) \cdot \sigma^2_{K_{2_e}} \end{aligned} \tag{17}$$

On the other hand, the model uncertainty propagation is achieved using Monte Carlo simulations, similar to those described in Sec. V-B, but with the generation of complete sets of signals for each window, in order to evaluate the uncertainty of the reconstructed signal for every sample of the signal. As shown in the example reported in Fig. 9, the model uncertainty will be larger towards the boundaries of the window, where the difference between the actual (instantaneous) and estimated (average) values of amplitude and phase are likely to be greater. For this reason, the model uncertainty is likely to be the largest contribution at the boundaries of the window.

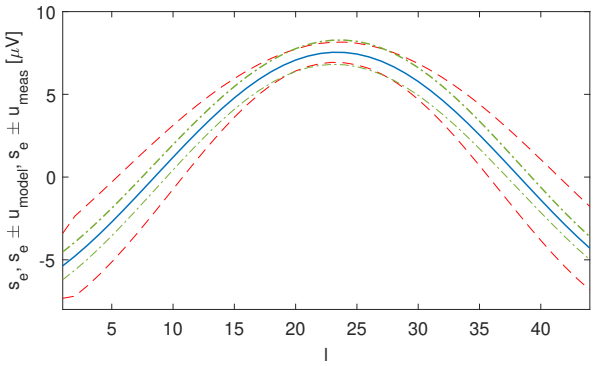

Fig. 9. Example of reconstructed signal in a window (blue line), with its model (red dashed line) and measurement (green dot-dashed line) uncertainty bands.

B. Compatibility verification and signal classification

Once the reconstructed signal $s_e(t)$ and its uncertainty have been calculated, the compatibility analysis can be performed, calculating how many points of the original signal, with their uncertainties, fall within the range defined by the reconstructed signal and its total uncertainty band. If all the samples in the window were uncorrelated, and assuming a Gaussian distribution, a percentage of 95% would correspond to a compatibility verified at 2σ level. However, there is a degree of correlation among samples, as already discussed, which affects the selection of a threshold for the signal classification. The effect of the correlation has been numerically evaluated via a Monte Carlo simulation and a threshold of 90% has been empirically determined as a more robust choice for a 2σ-level compatibility.

All the windows with at least 90% of the samples falling within the uncertainty band around the reconstructed signal are considered as carrying genuine alpha information, in agreement with the model assumptions. On the contrary, the other windows may be affected by artifacts or non-alpha components. This procedure can provide a first discrimination to identify the meaningful parts of the measured signal. In addition, the phase information can also help in the discrimination by evaluating the phase variation from window to window, but this will not be discussed further because it is out of the scope of this work.

VII. Results

The whole procedure described in previous sections has been applied to EEG acquisitions from two healthy subjects. Detailed results are reported and discussed in this section, focusing on a signal acquired from the occipital area (channel O2) of a male adult (Subject 1), while results from other channels and the other subject are summarized at the end of the section. Channel O2 has been chosen for this detailed analysis because the alpha activity is expected to be dominant in the occipital area, but the method can be applied to other channels as well.

For each subject and each channel, a first signal is used for calibration purposes, to estimate the alpha frequency, the

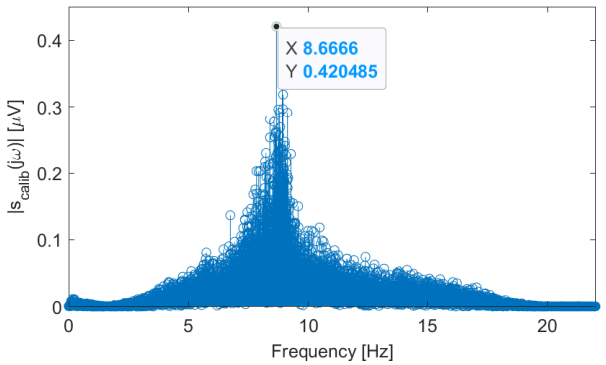

Fig. 10. Frequency spectrum of a 5-minute filtered calibration signal, showing the peak at the alpha frequency.

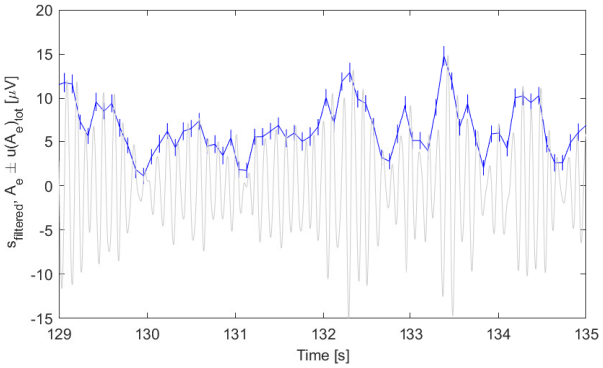

Fig. 11. Extract of filtered measured signal (gray line), with the estimated amplitudes and their total uncertainty bars (blue lines).

model parameters, and the uncertainties; the signal is acquired for 5 minutes in closed-eyes condition, in which alpha waves are more visible. The average alpha frequency is estimated by applying the Fourier Transform to the whole signal and identifying the frequency corresponding to the highest peak, illustrated in Fig. 10. In this case, the alpha frequency value is 8.7 Hz, which leads to an optimal window length of 44, corresponding to a time resolution of 88 ms in the amplitude and phase estimation (slightly shorter than the period of the alpha wave, i.e. 115 ms). It is worth noting that, although this may not be the most accurate method to estimate the alpha frequency, a very accurate estimate is not essential for the following steps, as shown below.

The information obtained from the calibration signal is then applied to a separate signal, recorded from the same subject and the same channel. In this case, the acquisition lasted for 10 minutes, the first 5 minutes with closed eyes and the last 5 minutes with open eyes. An extract from this signal, reasonably free from artifacts, is shown in Fig. 11, together with the estimated amplitudes and their uncertainties, window by window. The estimation of the amplitudes follows the oscillation of the original signal, while the uncertainty analysis provides a reasonably small bar within each window. On the overall signal, the mean value of the amplitude uncertainty is around 0.5 μV. For the avoidance of doubt, this uncertainty is calculated under the assumptions presented in the previous sections and, therefore, it does not include any effect of artifacts or other disturbances. The presence of artifacts is detected after the uncertainty calculation, by the compatibility analysis, and will invalidate the calculated uncertainty in the specific windows where the artifacts are detected.

To confirm the robustness of the proposed method against possible errors in the estimation of the alpha frequency, the window-by-window amplitude of the same signal has been estimated again, changing the alpha frequency value by $\pm$0.5 Hz. Such a large error is considered to be an extreme case, as the frequency estimate is likely to have a smaller uncertainty in most practical scenarios. The difference in the estimated amplitudes is less than the amplitude uncertainty in 99.3 % of the windows when the frequency error is +0.5 Hz, and in 99.2 % of the windows when the frequency error is -0.5 Hz. This shows that even a large frequency error of 0.5 Hz has a small impact on the amplitude estimation. Similar results are obtained also for other channels and the other subject, as shown in Table I.

The compatibility analysis explained in the previous section is then applied to discriminate between parts of the signal that are more likely to represent genuine alpha activity and those more likely to be affected by non-alpha components. Two extracts from the signal (both taken from the closed-eyes part) are reported in Fig. 12 and Fig. 13. In order to independently assess whether the filtered signal could be affected by non-alpha components, a time-frequency analysis of the unfiltered signal (filtered only by the IIR high-pass filter) is shown too: the amplitude spectrum is calculated by applying the FFT on windows of 0.5 s (leading to a frequency resolution of 2 Hz), in the range [2 20] Hz, whose components can partially pass through the FIR filter, with an attenuation of less than 40 dB (see Fig. 2). This result is compared to the compatibility analysis, performed on the much shorter window length L_{opt} (88 ms). The extract in Fig. 12 contains a dominant alpha wave, with no other significant component; in agreement with this, the compatibility is higher than 90 % in all windows (it is 100 % in most of them). On the contrary, the extract in Fig. 13 has visible lower-frequency components in the interval around 93-96 s, where the compatibility drops well below 90 % for most windows. The proposed method is, therefore, able to correctly recognize non-alpha components, despite being partially filtered by the band-pass filter, with the advantage of a much thinner time resolution, compared to the FFT analysis.

To summarize the results for the entire signal, including both closed-eyes and open-eyes intervals, the signal has been divided into segments of 5.016 s (each containing 57 windows of length L_{opt}); for each segment, the FFT is applied to the unfiltered signal to calculate the ratio between the power in the alpha band and the power in the [2 20] Hz range, and this index is compared to the number of compatible windows in that segment, according to the criterion defined in Sec. VI (compatibility $\geq$ 90 %). A scatter plot of the results is shown in Fig. 14. All segments with a dominant alpha power (i.e. where the alpha power is more than half of the total power in the [2 20] Hz band) have at least 94 % of compatible windows,

TABLE I
SUMMARY OF RESULTS FROM EXPERIMENTAL TESTS ON TWO HEALTHY SUBJECTS

Subject (sex, age)	Channel	Alpha frequency	L_{opt} (time)	Mean A_e	Mean $u(A_e)$	Perc. of windows where $e(A_e) < u(A_e)$ with ± 0.5 Hz error in f_α	Min. perc. of compatible windows in 5 s segments where $P_\alpha / P_{2-20} > 0.5$
Subject 1 (male, 35)	O2	8.67 Hz	44 (88 ms)	6.13 μV	0.53 μV	99.3 %, 99.2 %	94 %
	C3	8.67 Hz	45 (90 ms)	4.93 μV	0.43 μV	99.2 %, 99 %	96 %
Subject 2 (female, 33)	O1	11.05 Hz	36 (72 ms)	3.19 μV	0.35 μV	99.9 %, 99.9 %	100 %
	C4	11.25 Hz	36 (72 ms)	2.65 μV	0.29 μV	99.9 %, 99.9 %	98 %

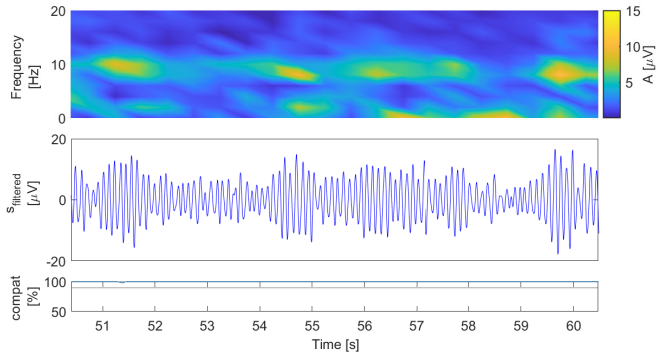

Fig. 12. First signal extract: amplitude spectrum of the unfiltered signal vs. time (top plot), filtered signal (middle plot), and compatibility check (bottom plot). All windows are compatible, i.e. their compatibility level is above the 90 % threshold (black line).

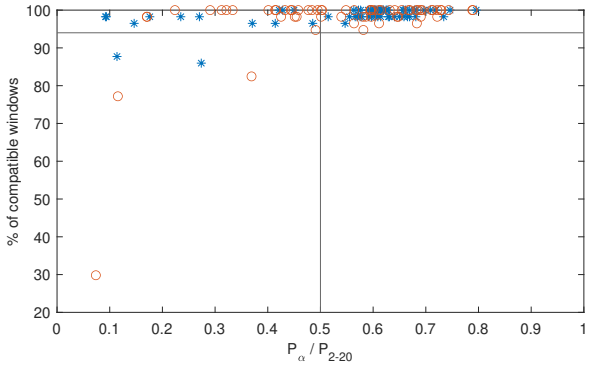

Fig. 14. Percentage of compatible windows within 5 s signal segments, as a function of the power ratio between the alpha band and the [2 20] Hz band in the unfiltered signal. The blue stars and red circles refer to the closed-eyes and open-eyes intervals of the signal, respectively. The 0.5 threshold is used to identify segments where the alpha power is dominant.

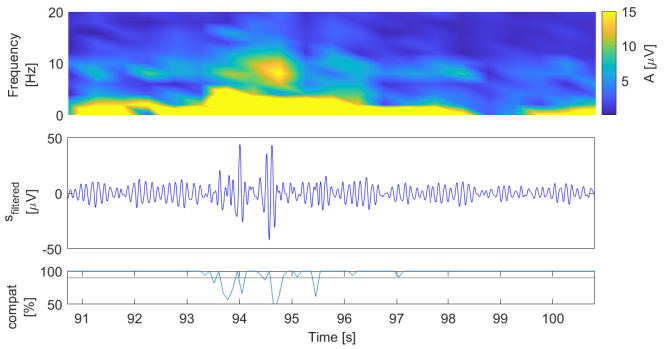

Fig. 13. Second signal extract: amplitude spectrum of the unfiltered signal vs. time (top plot), filtered signal (middle plot), and compatibility check (bottom plot). Many windows are below the 90 % compatibility threshold (black line).

whereas some of the other segments have a much lower percentage of compatible windows. This confirms that the proposed method correctly recognizes genuine alpha activity when there are no other significant components in the raw signal; on the other hand, the presence of other components may decrease the compatibility level, but not in all windows, meaning that some windows still contain signals that are compatible with genuine alpha activity, once filtered.

It should be noted that the analysis reported in Fig. 14 was applied to both closed-eyes and open-eyes parts of the signal, thus revealing that the calibration signal acquired with closed eyes remains relevant also to the open-eyes condition, despite the lower alpha amplitude. However, depending on the application and the subject, a calibration signal obtained in conditions more similar to the test condition may be preferred.

Similar tests, with the same procedure, were repeated on different subject and channels. The results are reported in Table I, together with the results from Subject 1 already presented. Besides the occipital channels, a central channel is also analyzed for each subject, to show that the method works well also in the presence of a weaker alpha signal. The average relative uncertainty of the estimated alpha amplitude is around 10 % for all tests, which is reasonably small, considering the challenges characterizing EEG measurements; however, it is important to remember that those uncertainty values are only valid within windows where the compatibility is verified, whereas they are likely to be much higher in the other windows. The ability to identify those different windows is one of the key benefits of the method proposed in this paper.

To test the effectiveness of the proposed method in more challenging conditions, additional tests were carried out with the subject performing head movements, which are known to cause artifacts in the EEG recordings, especially in the occipital area, closer to the neck. The results from Subject 1, channel O2, are reported in Fig. 15, where the first half of the signal was recorded in still conditions, while the second half was characterized by random head movements, detected by the accelerometer included in the EEG acquisition unit. The number of compatible windows decreases very noticeably during the movement, and there is a good correlation between the acceleration peaks and the non-compatible windows. An advantage of the proposed method is that it can still detect genuine alpha information in short good windows, even if the recording is affected by frequent movement.

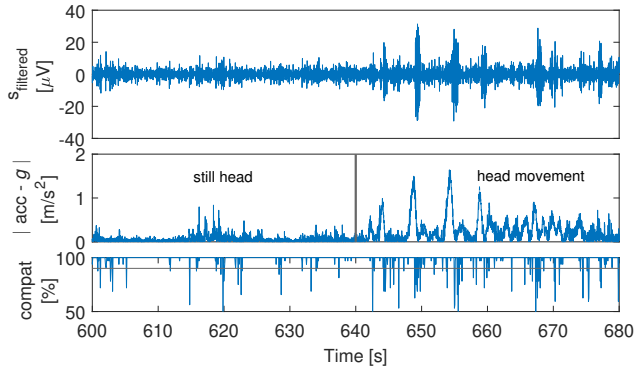

Fig. 15. Comparison of method performance in still condition (first half of the recording) and during head movements (second half): filtered signal (top plot), acceleration after baseline removal (middle plot), and compatibility check (bottom plot).

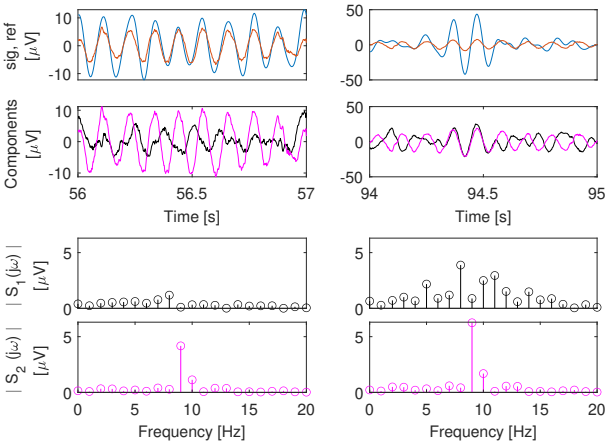

Fig. 16. The upper plots show the two sections of the signal (1 s each) used for the ICA: the blue lines are the measured signals, while the red ones are the references. The other plots show the two components identified by the ICA, in the time and frequency domains. The second component (magenta) is the one proportional to the reference, thus interpreted as alpha.

VIII. Comparison with Constrained ICA by Temporal Decorrelation

ICA is a common method used within the biomedical signal processing, and in particular EEG processing, when it is required to separate independent signal components, i.e. different bands or artifacts. Generally, in the formulation of the ICA, the observed signals $\mathbf{x}(t)$ are assumed to be a linear combination of unknown underlying independent sources $\mathbf{s}(t)$, described by the model in (18):

$$\mathbf{x}(t) = \mathbf{W} \cdot \mathbf{s}(t) \tag{18}$$

where $\mathbf{W}$ is the mixing matrix.

The aim of the ICA is to recover the sources $\mathbf{s}(t)$ directly from the observations $\mathbf{x}(t)$, through the identification of a de-mixing matrix $\mathbf{V}$:

$$\hat{\mathbf{s}}(t) = \mathbf{V} \cdot \mathbf{x}(t) \tag{19}$$

where $\hat{\mathbf{s}}(t)$ are the estimated sources.

There are several possible criteria that can be used to identify the de-mixing matrix $\mathbf{V}$. Here, the temporal decorrelation is chosen because it allows introducing some theoretical information about the signal, consistent with the alpha wave model described in Sec. II [39]. Thus, it is an appropriate comparison for the method proposed in this paper.

The temporal decorrelation approach is based on the assumption that the independent sources have no temporal correlation. A stack of cross-covariance matrices of the observed signals, $\mathbf{C}_x^\tau$, is defined for a set of time delays τ, while the cross-covariance matrices of the sources, $\mathbf{C}_s^\tau$, are a stack of diagonal matrices, due to the assumed source independence. Therefore, the de-mixing matrix $\mathbf{V}$ is a matrix that diagonalizes all matrices $\mathbf{C}_x^\tau$:

$$\mathbf{C}_s^\tau = \mathbf{V} \cdot \mathbf{C}_x^\tau \cdot \mathbf{V}^T \tag{20}$$

Although the ICA is a blind source separation technique, it is possible to constrain the separation process by introducing *a priori* information on the sources. This can be done by adding an artificial reference signal $r(t)$ to the measured signal $x(t)$, with similar characteristics to one of the expected sources:

$$\tilde{\mathbf{x}}(t) = \begin{bmatrix} x(t) \\ r(t) \end{bmatrix} \tag{21}$$

The addition of a reference signal allows also expanding the number of sources that can be identified and, therefore, it allows the application of ICA to a single-channel EEG. In this case, a simple solution is obtained by choosing one of the two sources equal to the reference signal. For the purpose of alpha wave identification, the reference signal is the simulated alpha wave, generated by the model identified from the calibration signal, but with the alpha frequency estimated from the considered signal and with no phase modulation. To avoid the issues caused by the random phase of the reference signal, the cross-covariance matrices described above can be calculated in the frequency domain, by removing the phase difference between the measured and reference signals, as done in [39].

This ICA method has been applied to the same filtered signal extracts shown in Figs. 12 and 13, but on shorter time windows of 1 s. The short windows are required by the assumption of stationarity of the sources, which is unlikely to be valid on long windows. Both the filtered and reference signals are reported in Fig. 16, together with the two signal components identified by the ICA, in both time and frequency domains. For the first signal extract (left), which is believed to be mostly a pure alpha signal based on the analysis from the previous section, the component proportional to the reference is the dominant one; on the other hand, for the second signal extract (right), which is affected by significant non-alpha disturbances, the component proportional to the reference is not dominant and it is not a good fit with the measured signal in most of the window.

Although this ICA analysis can broadly distinguish between windows with genuine alpha signals and windows with significant non-alpha components, it has some important disadvantages compared to the proposed method: 1) the time window for the analysis must be longer, thus leading to a worse time resolution; 2) it is less robust with respect to errors in the alpha frequency used in the model; 3) it does not allow a straightforward uncertainty evaluation.

IX. Conclusion

This work aimed to address one of the main challenges in EEG signal processing, i.e. the reliable identification of specific features (in this case, alpha oscillations) from signals that are likely to be affected by artifacts and other disturbances. While several methods in time, frequency, and time-frequency domains have been presented in the literature, the uncertainty analysis has been under-investigated and it is proposed in this paper as a suitable tool to allow a metrology-sound approach for the identification of alpha waves, based on the compatibility between the measured signal and its model-based expectation.

In more detail, this paper used a time-domain fitting method to extract the alpha amplitude oscillation from single-channel EEG signals, based on a mathematical model of the alpha wave, whose parameters can be identified for each subject from a calibration signal. A fundamental advantage of this approach is the ability to quantify the uncertainties arising from both measurement and model, which allows not only optimizing the estimation accuracy of the alpha amplitude but more importantly, also verifying *a posteriori* if the measured signal and theoretical model are compatible with each other. Such a compatibility analysis provides a robust and conceptually rigorous tool to discriminate between parts of the signal that contain genuine alpha information and those affected by artifacts or other EEG components.

The proposed method has been successfully demonstrated on EEG signals acquired from two healthy subjects and compared to a more traditional time-frequency analysis, based on the Short-Time Fourier Transform, used to independently detect the presence of non-alpha components in the signal. While the two methods provided similar conclusions in most cases, a notable advantage of the proposed approach is that the time-domain fitting allows estimating the alpha amplitude with much thinner, sub-cycle resolution (i.e. less than one full cycle of the alpha wave), whereas the STFT requires a longer time window in order to achieve an acceptable frequency resolution. The optimal time resolution (or window of analysis) is tailored to the alpha frequency, which is known to vary from subject to subject.

Finally, the proposed method has been compared also to one of the most commonly used techniques in EEG signal processing, i.e. the Independent Component Analysis, in the form of constrained ICA by temporal decorrelation. Although it is more suitable for multi-channel applications, this technique was chosen because it employs a reference signal to introduce *a priori* information, similar to the model used in the proposed method, and thus it represents a meaningful comparison, albeit in a very simplified condition. In this scenario, the ICA is affected by similar limitations to the STFT, i.e. worse time resolution, worse robustness with respect to errors in the alpha frequency, and worse interpretability of the results due to the lack of straightforward uncertainty quantification.

In conclusion, the proposed method appears to be promising and deserves further investigation with larger data sets. In particular, its use is encouraged in those applications requiring high reliability, such as clinical studies and certain types of brain-machine interfaces, where a wrong interpretation of signal features can have potentially serious consequences.

References

[1] J. S. Kumar and P. Bhuvaneswari, "Analysis of electroencephalography (eeg) signals and its categorization–a study," *Procedia engineering*, vol. 38, pp. 2525–2536, 2012.

[2] M. Soufineyestani, D. Dowling, and A. Khan, "Electroencephalography (eeg) technology applications and available devices," *Applied Sciences*, vol. 10, no. 21, p. 7453, 2020.

[3] V. Nandikolla, B. Ghoslin, K. Matsuno, and D. A. Medina Portilla, "A brain-computer interface for teleoperation of a semiautonomous mobile robotic assistive system using slam," *Journal of Robotics*, vol. 2022, 2022.

[4] A. Khosla, P. Khandnor, and T. Chand, "A comparative analysis of signal processing and classification methods for different applications based on eeg signals," *Biocybernetics and Biomedical Engineering*, vol. 40, no. 2, pp. 649–690, 2020.

[5] P. A. d. M. Kanda, R. Anghinah, M. T. Smidth, and J. M. Silva, "The clinical use of quantitative eeg in cognitive disorders," *Dementia & Neuropsychologia*, vol. 3, no. 3, pp. 195–203, 2009.

[6] S.-P. Seo, M.-H. Lee, J. Williamson, and S.-W. Lee, "Changes in fatigue and eeg amplitude during a longtime use of brain-computer interface," in *2019 7th International Winter Conference on Brain-Computer Interface (BCI)*, 2019, pp. 1–3.

[7] J. Carp and R. J. Compton, "Alpha power is influenced by performance errors," *Psychophysiology*, vol. 46, no. 2, pp. 336–343, 2009.

[8] C. Brunner, A. Delorme, and S. Makeig, "Eeglab–an open source matlab toolbox for electrophysiological research," *Biomedical Engineering/Biomedizinische Technik*, vol. 58, no. SI-1-Track-G, 2013.

[9] J. A. Urigüen and B. Garcia-Zapirain, "Eeg artifact removal—state-of-the-art and guidelines," *Journal of neural engineering*, vol. 12, no. 3, p. 031001, 2015.

[10] R. Vigario and E. Oja, "Bss and ica in neuroinformatics: from current practices to open challenges," *IEEE reviews in biomedical engineering*, vol. 1, pp. 50–61, 2008.

[11] C. J. James and S. Wang, "Blind source separation in single-channel eeg analysis: An application to bci," in *2006 International Conference of the IEEE Engineering in Medicine and Biology Society*. IEEE, 2006, pp. 6544–6547.

[12] M. Davies and C. James, "Source separation using single channel ica," *Signal Processing*, vol. 87, no. 8, pp. 1819–1832, 2007.

[13] A. K. Maddirala and R. A. Shaik, "Separation of sources from single-channel eeg signals using independent component analysis," *IEEE Transactions on Instrumentation and measurement*, vol. 67, no. 2, pp. 382–393, 2017.

[14] B. Azzerboni, F. La Foresta, N. Mammone, and F. C. Morabito, "A new approach based on wavelet-ica algorithms for fetal electrocardiogram extraction." in *ESANN*. Citeseer, 2005, pp. 193–198.

[15] C.-Y. Chang, S.-H. Hsu, L. Pion-Tonachini, and T.-P. Jung, "Evaluation of artifact subspace reconstruction for automatic artifact components removal in multi-channel eeg recordings," *IEEE Transactions on Biomedical Engineering*, vol. 67, no. 4, pp. 1114–1121, 2019.

[16] X. Chen, Z. J. Wang, and M. McKeown, "Joint blind source separation for neurophysiological data analysis: Multiset and multimodal methods," *IEEE Signal Processing Magazine*, vol. 33, no. 3, pp. 86–107, 2016.

[17] X. Chen, H. Peng, F. Yu, and K. Wang, "Independent vector analysis applied to remove muscle artifacts in eeg data," *IEEE Transactions on Instrumentation and Measurement*, vol. 66, no. 7, pp. 1770–1779, 2017.

[18] A. Liu, G. Song, S. Lee, X. Fu, and X. Chen, "A state-dependent iva model for muscle artifacts removal from eeg recordings," *IEEE Transactions on Instrumentation and Measurement*, vol. 70, pp. 1–13, 2021.

[19] F. Morbidi, A. Garulli, D. Prattichizzo, C. Rizzo, and S. Rossi, "Application of kalman filter to remove tms-induced artifacts from eeg recordings," *IEEE Transactions on Control Systems Technology*, vol. 16, no. 6, pp. 1360–1366, 2008.

[20] J. Kaur and A. Kaur, "A review on analysis of eeg signals," in *2015 International Conference on Advances in Computer Engineering and Applications*. IEEE, 2015, pp. 957–960.

[21] C. Zhang and A. Eskandarian, "A survey and tutorial of eeg-based brain monitoring for driver state analysis," *IEEE/CAA Journal of Automatica Sinica*, vol. 8, no. 7, pp. 1222–1242, 2021.

[22] M. Huang, P. Wu, Y. Liu, L. Bi, and H. Chen, "Application and contrast in brain-computer interface between hilbert-huang transform and wavelet transform," in *2008 The 9th International Conference for Young Computer Scientists*. IEEE, 2008, pp. 1706–1710.
[23] A. Médl, D. Flotzinger, and G. Pfurtscheller, "Hilbert-transform based predictions of hand movements from eeg measurements," in *1992 14th Annual International Conference of the IEEE Engineering in Medicine and Biology Society*, vol. 6. IEEE, 1992, pp. 2539–2540.
[24] M. A. Platas-Garza and J. A. de la O Serna, "Dynamic harmonic analysis through taylor–fourier transform," *IEEE Transactions on Instrumentation and Measurement*, vol. 60, no. 3, pp. 804–813, 2010.
[25] N. Hazarika, J. Z. Chen, A. C. Tsoi, and A. Sergejew, "Classification of eeg signals using the wavelet transform," *Signal processing*, vol. 59, no. 1, pp. 61–72, 1997.
[26] M.-P. Hosseini, A. Hosseini, and K. Ahi, "A review on machine learning for eeg signal processing in bioengineering," *IEEE reviews in biomedical engineering*, vol. 14, pp. 204–218, 2020.
[27] A. E. Alchalabi, S. Shirmohammadi, A. N. Eddin, and M. Elsharnouby, "Focus: Detecting adhd patients by an eeg-based serious game," *IEEE Transactions on Instrumentation and Measurement*, vol. 67, no. 7, pp. 1512–1520, 2018.
[28] C. Ieracitano, N. Mammone, A. Hussain, and F. C. Morabito, "A novel multi-modal machine learning based approach for automatic classification of eeg recordings in dementia," *Neural Networks*, vol. 123, pp. 176–190, 2020.
[29] U. R. Acharya, H. Fujita, V. K. Sudarshan, S. Bhat, and J. E. Koh, "Application of entropies for automated diagnosis of epilepsy using eeg signals: A review," *Knowledge-based systems*, vol. 88, pp. 85–96, 2015.
[30] A. Lay-Ekuakille, P. Vergallo, G. Griffo, F. Conversano, S. Casciaro, S. Urooj, V. Bhateja, and A. Trabacca, "Entropy index in quantitative eeg measurement for diagnosis accuracy," *IEEE Transactions on Instrumentation and Measurement*, vol. 63, no. 6, pp. 1440–1450, 2013.
[31] Z. Liang, Y. Wang, X. Sun, D. Li, L. J. Voss, J. W. Sleigh, S. Hagihira, and X. Li, "Eeg entropy measures in anesthesia," *Frontiers in computational neuroscience*, vol. 9, p. 16, 2015.
[32] "Evaluation of Measurement Data—Guide to the Expression of Uncertainty in Measurement, (GUM 1995 With Minor Corrections)," Joint Committee for Guides in Metrology, document JCGM 100:2008, 2008.
[33] S. Shirmohammadi, K. Barbe, D. Grimaldi, S. Rapuano, and S. Grassini, "Instrumentation and measurement in medical, biomedical, and healthcare systems," *IEEE Instrumentation & Measurement Magazine*, vol. 19, no. 5, pp. 6–12, 2016.
[34] M. Parvis and A. Vallan, "Medical measurements and uncertainties," *IEEE Instrumentation & Measurement Magazine*, vol. 5, no. 2, pp. 12–17, 2002.
[35] R. Leca and V. Groza, "On the need to estimate the adequacy of measurement results," in *2009 IEEE International Workshop on Advanced Methods for Uncertainty Estimation in Measurement*, 2009, pp. 1–4.
[36] M. A. Schier, "Changes in eeg alpha power during simulated driving: a demonstration," *International Journal of Psychophysiology*, vol. 37, no. 2, pp. 155–162, 2000.
[37] V. Casadei, R. Ferrero, and C. Brown, "Model-based filtering of eeg alpha waves for enhanced accuracy in dynamic conditions and artifact detection," in *2020 IEEE International Instrumentation and Measurement Technology Conference (I2MTC)*. IEEE, 2020, pp. 1–6.
[38] Grandy, Thomas H and Werkle-Bergner, Markus and Chicherio, Christian and Schmiedek, Florian and Lövdén, Martin and Lindenberger, Ulman, "Peak individual alpha frequency qualifies as a stable neurophysiological trait marker in healthy younger and older adults," *Psychophysiology*, vol. 50, no. 6, pp. 570–582, 2013.
[39] C. J. James and C. W. Hesse, "Independent component analysis for biomedical signals," *Physiological measurement*, vol. 26, no. 1, p. R15, 2004.

Valentina Casadei (S'18) received her Master's degree in Biomedical Engineering from Università Politecnica delle Marche, Italy, in 2019. She is currently pursuing her Ph.D. in Electrical Engineering at the University of Liverpool, UK. Her thesis focuses on a metrology-sound approach for the analysis of wearable biomedical signals to improve their reliability and interpretation.

Roberto Ferrero (S'10-M'14-SM'18) received his PhD degree (*cum laude*) in Electrical Engineering from Polytechnic of Milan, Italy, in 2013. From 2015 to 2019 he was a Lecturer with the Department of Electrical Engineering and Electronics, University of Liverpool, UK, where he is currently a Senior Lecturer (Associate Professor). His main research activity is focused on electrical measurements, particularly applied to power systems, electrochemical devices and wearable sensors.

Dr. Ferrero is a member of the IEEE Instrumentation and Measurement Society, and of its TC 39 (Measurements in Power Systems). He has been an Associate Editor-in-Chief of the IEEE Transactions on Instrumentation and Measurement since 2021 (previously Associate Editor since 2017), currently with the role of Senior Area Editor for Power Instrumentation and Measurement.